Seg1 controls eisosome assembly and shape

Karen E. Moreira,[1] Sebastian Schuck,[1] Bianca Schrul,[2,3] Florian Fröhlich,[4] James B. Moseley,[5] Tobias C. Walther,[4] and Peter Walter[1]

[1]Howard Hughes Medical Institute and Department of Biochemistry and Biophysics, University of California San Francisco, San Francisco, CA 94158
[2]Department of Biochemistry I, University Medical Center, Georg-August University Göttingen, 37073 Göttingen, Germany
[3]Max Planck Institute for Biophysical Chemistry, 37077 Göttingen, Germany
[4]Department of Cell Biology, Yale University School of Medicine, New Haven, CT 06520
[5]Department of Biochemistry, Geisel School of Medicine at Dartmouth, Hanover, NH 03755

Eisosomes are stable domains at the plasma membrane of the budding yeast *Saccharomyces cerevisiae* and have been proposed to function in endocytosis. Eisosomes are composed of two main cytoplasmic proteins, Pil1 and Lsp1, that form a scaffold around furrow-like plasma membrane invaginations. We show here that the poorly characterized eisosome protein Seg1/Ymr086w is important for eisosome biogenesis and architecture. Seg1 was required for efficient incorporation of Pil1 into eisosomes and the generation of normal plasma membrane furrows. Seg1 preceded Pil1 during eisosome formation and established a platform for the assembly of other eisosome components. This platform was further shaped and stabilized upon the arrival of Pil1 and Lsp1. Moreover, Seg1 abundance controlled the shape of eisosomes by determining their length. Similarly, the *Schizosaccharomyces pombe* Seg1-like protein Sle1 was necessary to generate the filamentous eisosomes present in fission yeast. The function of Seg1 in the stepwise biogenesis of eisosomes reveals striking architectural similarities between eisosomes in yeast and caveolae in mammals.

Introduction

Cells subdivide their plasma membrane into regions with specialized functions. One way to achieve this compartmentalization is to construct diffusion barriers within the plasma membrane and furnish the resulting surface domains with unique compositions by means of dedicated membrane trafficking pathways (Nakada et al., 2003; Schuck and Simons, 2004; Caudron and Barral, 2009; Steed et al., 2010). Another way to segregate plasma membrane components is based on the propensity of certain lipids, namely sterols and sphingolipids, to form microdomains by preferential association (Lingwood and Simons, 2010). These microdomains, called lipid rafts, can be clustered into larger assemblies by specialized protein scaffolds. Mammalian scaffolding proteins of this type are the caveolins. These integral membrane proteins bind cholesterol, polymerize into stable protein lattices, and shape the plasma membrane into 60–80-nm-deep cup-like caveolae that serve as sites of clathrin-independent endocytosis (Parton and Simons, 2007; Hansen and Nichols, 2009; Bastiani and Parton, 2010).

The yeast *Saccharomyces cerevisiae* possesses plasma membrane domains that share many fundamental features with caveolae (Ziółkowska et al., 2012). Their principal protein components are Pil1 and Lsp1, two highly similar cytoplasmic proteins that are each present at an abundance of ∼100,000 copies per cell (Ghaemmaghami et al., 2003). The two proteins bind to one another and generate 20–50 immobile plasma membrane-associated assemblies in every cell, with each assembly containing on the order of 2,000–5,000 subunits of both Pil1 and Lsp1 (Walther et al., 2006). Pil1/Lsp1 assemblies are evenly distributed over the plasma membrane and maintain a minimal distance from each other (Moreira et al., 2009). The sites at which Pil1/Lsp1 associate with the plasma membrane correspond to furrow-like membrane invaginations that are ∼50 nm deep and 200–300 nm long (Strádalová et al., 2009). These invaginated membrane patches appear to be enriched in ergosterol, the major yeast sterol (Grossmann et al., 2007), and they require sphingolipids for proper organization (Grossmann et al., 2006; Fröhlich et al., 2009). Pil1/Lsp1 have been suggested to participate in

K.E. Moreira and S. Schuck contributed equally to this paper.
Correspondence to Peter Walter: peter@walterlab.ucsf.edu

© 2012 Moreira et al. This article is distributed under the terms of an Attribution–Noncommercial–Share Alike–No Mirror Sites license for the first six months after the publication date (see http://www.rupress.org/terms). After six months it is available under a Creative Commons License (Attribution–Noncommercial–Share Alike 3.0 Unported license, as described at http://creativecommons.org/licenses/by-nc-sa/3.0/).

The Rockefeller University Press $30.00
J. Cell Biol. Vol. 198 No. 3 405–420
www.jcb.org/cgi/doi/10.1083/jcb.201202097

endocytosis, but this connection remains to be clarified (Walther et al., 2006; Grossmann et al., 2008; Brach et al., 2011).

The Pil1/Lsp1 assemblies have been named "eisosomes" (Walther et al., 2006), whereas the ergosterol-enriched membrane patches that colocalize with Pil1/Lsp1 have been called "membrane compartment of arginine permease Can1" (MCC; Malínská et al., 2003, 2004; Grossmann et al., 2008; Malínsky et al., 2010). The terms eisosome and MCC likely describe connected parts of the same cellular structure. First, in cells lacking Pil1, MCC-associated transmembrane proteins disperse in the plasma membrane and furrow-like invaginations disappear (Walther et al., 2006; Grossmann et al., 2007, 2008; Fröhlich et al., 2009; Strádalová et al., 2009). The integrity of the MCC therefore depends on the eisosome protein Pil1. Second, disruption of the MCC, for example by sphingolipid depletion, is relayed to Pil1 by phosphorylation, and causes a large fraction of Pil1 to dissociate from the plasma membrane (Walther et al., 2007; Luo et al., 2008; Fröhlich et al., 2009). The integrity of eisosomes therefore depends on an intact MCC. Third, Pil1 and Lsp1 both contain membrane-shaping BAR domains, bind to liposomes in vitro, and self-assemble into filaments whose dimensions match those of plasma membrane furrows in vivo (Karotki et al., 2011; Olivera-Couto et al., 2011; Ziółkowska et al., 2011). Eisosome components in cells are therefore likely to directly interact with and scaffold the plasma membrane. In view of these links, we suggest treating the whole subcellular structure as a single entity, consisting of a furrow-like plasma membrane domain, the transmembrane proteins that partition into this domain, and the proteins that form a scaffolding lattice on its cytoplasmic face. In this paper, we shall use the term eisosome in this sense.

The proper assembly of eisosomes critically depends on Pil1. In its absence, Lsp1 is mostly cytoplasmic, whereas Pil1 retains its normal distribution in cells lacking Lsp1 (Walther et al., 2006). Furthermore, without Pil1, eisosome components partially collapse into a small number of clusters, referred to as eisosome remnants (Walther et al., 2006; Grossmann et al., 2007). Eisosome remnants correspond to large aberrant plasma membrane invaginations (Walther et al., 2006; Strádalová et al., 2009). Reducing or raising the levels of Pil1 yields a lower number of normal eisosomes or a normal number of larger eisosomes, respectively (Moreira et al., 2009). These observations indicate that there is a lower limit for eisosome size and an upper limit for eisosome number. The molecular mechanisms imposing these limits are unknown.

To better understand the architecture and ultimately the function of eisosomes, we have previously conducted a screen to identify genes involved in eisosome formation (Fröhlich et al., 2009). Several of the identified genes had no known function. Here, we study one of these poorly characterized genes, YMR086W, which encodes a large coiled-coil protein without recognizable functional domains. Based on the observation that its homologue in the yeast *Ashbya gossypii* is important for eisosome stability, YMR086W has been named *SEG1* for "stability of eisosomes guaranteed" (Seger et al., 2011). We find that the Seg1 protein facilitates eisosome assembly and controls eisosome shape.

Results

Seg1 is required for proper eisosome architecture

Our previous screen had shown that cells lacking Seg1 fail to properly localize Pil1-GFP, which indicates a defect in eisosome formation (Fröhlich et al., 2009). To analyze this phenotype in detail, we first imaged Pil1-GFP in wild-type and *seg1*Δ cells. In the absence of Seg1, cells displayed a reduced number of eisosomes, as defined by Pil1-GFP patches at the plasma membrane (Fig. 1 A). In addition, the Pil1-GFP signal of remaining eisosomes was decreased and the cytoplasmic Pil1-GFP signal was increased (Fig. 1 B). These findings show that Seg1 is required for efficient incorporation of Pil1-GFP into eisosomes.

Next, we analyzed the plasma membrane morphology of wild-type, *seg1*Δ, and *pil1*Δ cells by electron microscopy. Consistent with earlier studies (Moor and Mühlethaler, 1963; Strádalová et al., 2009), wild-type cells showed plasma membrane furrows ∼30 nm deep, 30 nm wide and 200 nm long (Fig. 1 C, left; see Fig. S1 A for serial sections). In contrast, s*eg1*Δ cells had deep, irregularly shaped plasma membrane invaginations (Fig. 1 C, middle and top right; see Fig. S1 B for serial sections). These invaginations were sometimes reminiscent of eisosome remnants seen in *pil1*Δ cells (Fig. 1 C, bottom right), but were generally smaller. These findings show that Seg1 is required for proper plasma membrane morphology. It appears likely that the aberrant invaginations observed in *seg1*Δ cells by electron microscopy correspond to the remaining Pil1-GFP patches seen in these cells by light microscopy. Collectively, Seg1 is needed for two aspects of eisosome architecture: the assembly of Pil1-GFP into membrane-associated complexes of characteristic size and the local molding of the plasma membrane into well-defined furrows.

Seg1 is an eisosome component

Seg1 has been shown to colocalize with Lsp1 and interact with Pil1/Lsp1 (Deng et al., 2009). Accordingly, Seg1-GFP colocalized with Pil1-cherry (Fig. 2 A). We next used immunogold labeling with an anti-GFP antibody to localize Seg1-GFP by immunoelectron microscopy. As expected, the immunogold marked plasma membrane invaginations characteristic of eisosomes (Fig. 2 B). Although the labeling was specific, its density was quite low, possibly because the GFP epitope is rendered largely inaccessible by the eisosomal protein lattice.

Using quantitative Western blotting, we compared the levels of Seg1, Pil1, and Lsp1 expressed as GFP fusions from their endogenous chromosomal loci and found that Seg1 is about 10-fold less abundant than Pil1 or Lsp1 (Fig. 2 C). Because a single eisosome contains 2,000–5,000 molecules of each Pil1 and Lsp1 (Walther et al., 2006), there are likely 200–500 Seg1 molecules per eisosome.

To identify Seg1 interaction partners, we quantitatively analyzed Seg1 immunoprecipitates using SILAC (stable isotope labeling with amino acids in cell culture). We immunopurified Seg1 from cells that expressed Seg1-TEV-GFP and had been metabolically labeled with heavy isotope lysine.

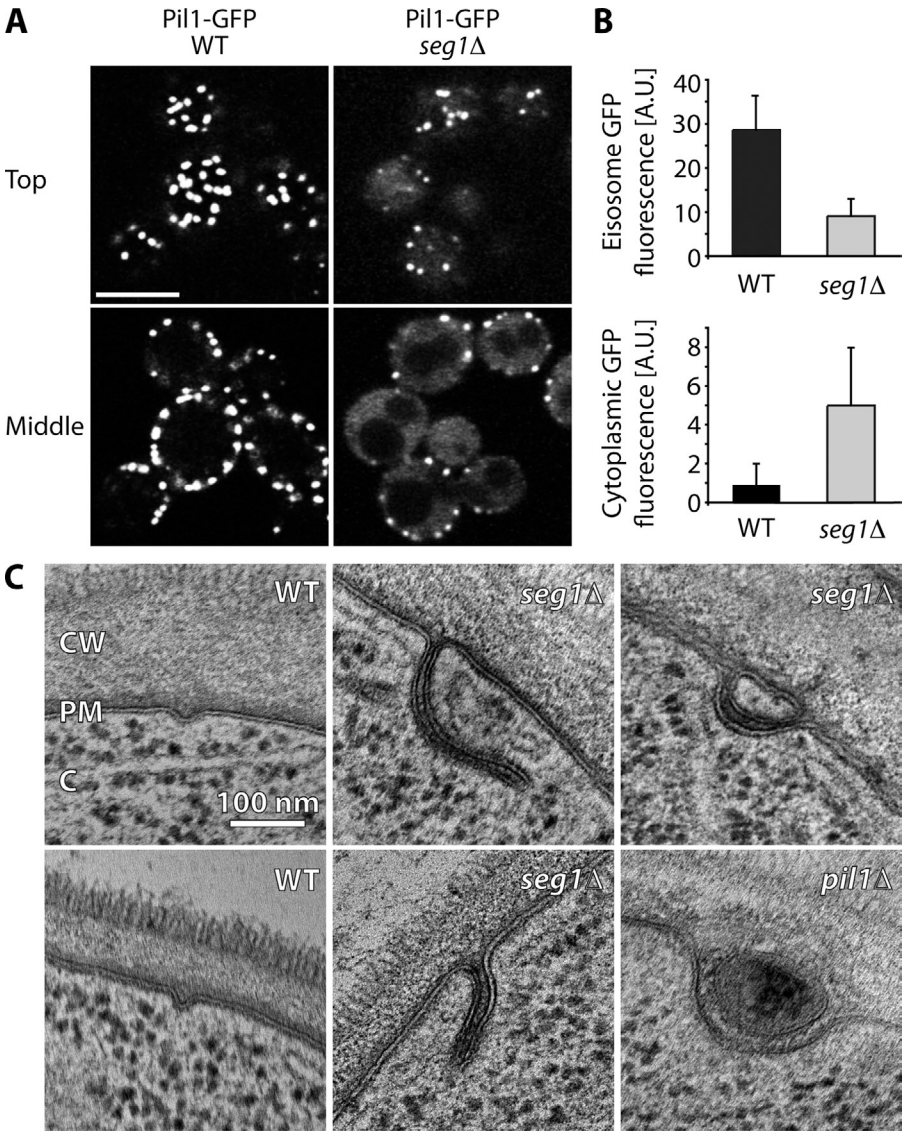

Figure 1. **Seg1 is required for proper eisosome architecture.** (A) Confocal images of Pil1-GFP in wild-type (WT) and *seg1Δ* cells. Representative top views and mid sections are shown. Bar, 5 µm. (B) Quantification of Pil1-GFP signal per eisosome (eisosome GFP fluorescence) and Pil1-GFP signal in the cytoplasm (cytoplasmic GFP fluorescence) in WT and *seg1Δ* cells. A.U., arbitrary units. Error bars indicate standard deviations. (C) Electron micrographs of WT, *seg1Δ*, and *pil1Δ* cells. CW, cell wall; PM, plasma membrane; C, cytoplasm.

The resulting eluate was mixed with that from a mock purification using untagged control cells grown in the presence of normal, light isotope lysine. Finally, the ratio of heavy/light lysine was determined for each protein identified by mass spectrometry. A high heavy/light ratio for a given protein indicates enrichment in the metabolically labeled sample and hence interaction with Seg1. By this measure, Seg1 interacts with the known eisosome proteins Pil1, Lsp1, Eis1/Ymr031c, and Ygr130c, as well as the Seg1 paralogue Seg2/Ykl105c (Fig. 2 D). These results confirm that Seg1 is an eisosome protein.

Seg1 precedes Pil1 during eisosome assembly

To begin to investigate the role of Seg1 in eisosome formation, we analyzed the incorporation of Seg1 into nascent eisosomes during yeast budding. Growing buds are initially devoid of eisosomes as marked by Pil1 and Lsp1. Once a bud exceeds a critical size, it is colonized by newly assembled eisosomes. Colonization occurs in a polarized fashion, starting from the bud neck (Moreira et al., 2009). However, when we imaged the deposition of Seg1, we observed Seg1-GFP already in small buds, where it was diffusely distributed and formed heterogeneous patches at the plasma membrane (Fig. 3 A, top). Medium-sized buds were evenly colonized by Seg1-GFP patches, whereas Pil1-GFP patches exhibited the characteristic polarized distribution observed previously (Fig. 3 A, middle). Large buds showed a uniform pattern for both Seg1-GFP and Pil1-GFP patches (Fig. 3 A, bottom). These observations indicate that Seg1 deposition precedes that of Pil1. We also attempted to image Seg1 and Pil1 in the same cells by fusing them to different fluorescent proteins. However, these experiments were rendered uninterpretable by the different maturation times of the fluorophores so that the protein fused to the faster maturing fluorescent protein always seemed to enter growing buds first. To refine our results, we quantified Seg1-GFP patches in buds of different sizes and plotted their number against bud surface area. Consistent with earlier measurements (Moreira et al., 2009), Pil1-GFP patches were absent in buds with a surface area <15 μm^2, showing a lag phase for Pil1 deposition (Fig. 3 B). In contrast, there was no lag

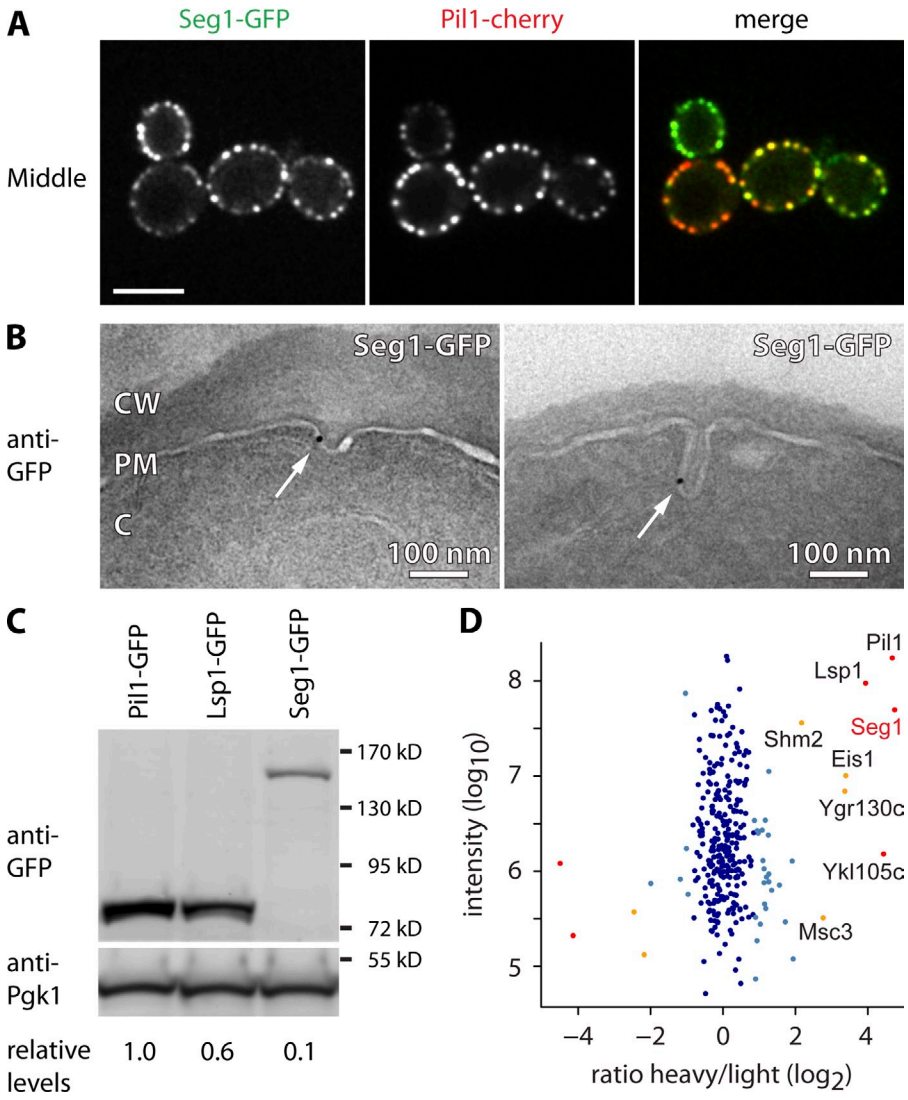

Figure 2. **Seg1 is an eisosome component.** (A) Confocal mid sections of cells expressing Seg1-GFP and Pil1-cherry. Bar, 5 µm. (B) Electron micrographs of Seg1-GFP cells labeled with anti-GFP antibody and gold-conjugated protein A. Arrows indicate gold particles. CW, cell wall; PM, plasma membrane; C, cytoplasm. (C) Western blot of GFP and Pgk1 from cells expressing Pil1-GFP, Lsp1-GFP, or Seg1-GFP from their endogenous loci. Numbers indicate GFP levels relative to Pgk1 and normalized to Pil1-GFP. (D) Mass spectrometric analysis of Seg1 affinity-purified from heavy-labeled cells expressing Seg1-TEV-GFP and light-labeled, untagged control cells. The averaged peptide intensity is plotted against the ratio of heavy/light. Significant outliers are colored in red ($P < 10^{-11}$), orange ($P < 10^{-4}$), or light blue ($P < 0.05$). Other identified proteins are colored in dark blue.

phase for the formation of Seg1-GFP patches, which indicates that deposition of Seg1 does not require a minimum bud size. These results confirm that Seg1 becomes part of eisosome precursors before the arrival of Pil1.

Seg1 facilitates eisosome assembly

The diffuse distribution of Seg1 in small buds lacking Pil1 suggested that uniform and stable assembly of Seg1 requires Pil1. To test this idea, we analyzed Seg1-GFP in *pil1Δ* cells. Consistent with Pil1 being critical for eisosome biogenesis, Seg1-GFP displayed an uneven distribution at the plasma membrane with a few remaining patches (Fig. 3 C, middle). Additional deletion of Lsp1 had no effect, nor did deletion of Lsp1 alone (Fig. 3 C, right; and not depicted).

Given that Seg1 has no predicted transmembrane domains, its plasma membrane association in *pil1Δ* cells and in small buds lacking Pil1 was unexpected. So far, eisosome proteins without transmembrane domains, such as Lsp1 and Pkh2, have been found mainly in the cytoplasm in the absence of Pil1 (Walther et al., 2006, 2007). We noticed that the C terminus of Seg1 contains clusters of basic residues (Fig. 4 C). To test if this region mediates plasma membrane association, we analyzed the localization of Seg1Δ942-GFP, which lacks the last 18 amino acids of Seg1. The truncated Seg1 localized mostly to eisosomes in wild-type cells, as judged by colocalization with Pil1-cherry (Fig. 4 A). In addition, cells expressing untagged Seg1Δ942 as the only copy of Seg1 had a normal steady-state distribution of Pil1-GFP (unpublished data). However, Seg1Δ942-GFP was completely cytoplasmic in *pil1Δ lsp1Δ* cells, demonstrating that the basic C terminus targets Seg1 to the plasma membrane in the absence of Pil1/Lsp1 (Fig. 4 B). To test directly if the C terminus of Seg1 is able to bind lipids, we fused it to GST and assayed binding of recombinant GST-Seg1(941–960) to liposomes of varying composition. GST-Seg1(941–960) showed binding to liposomes consisting exclusively of phosphatidylcholine, but binding was enhanced by addition of the negatively charged lipids phosphatidylinositol-(4,5)-bisphosphate (PIP_2), phosphatidylserine, or phosphatidic acid (Fig. 4 D). Therefore, the C terminus of Seg1 is sufficient to bind lipids, at least in vitro. We conclude that Seg1 is kept at the plasma membrane by two interactions. The first requires Pil1/Lsp1 and

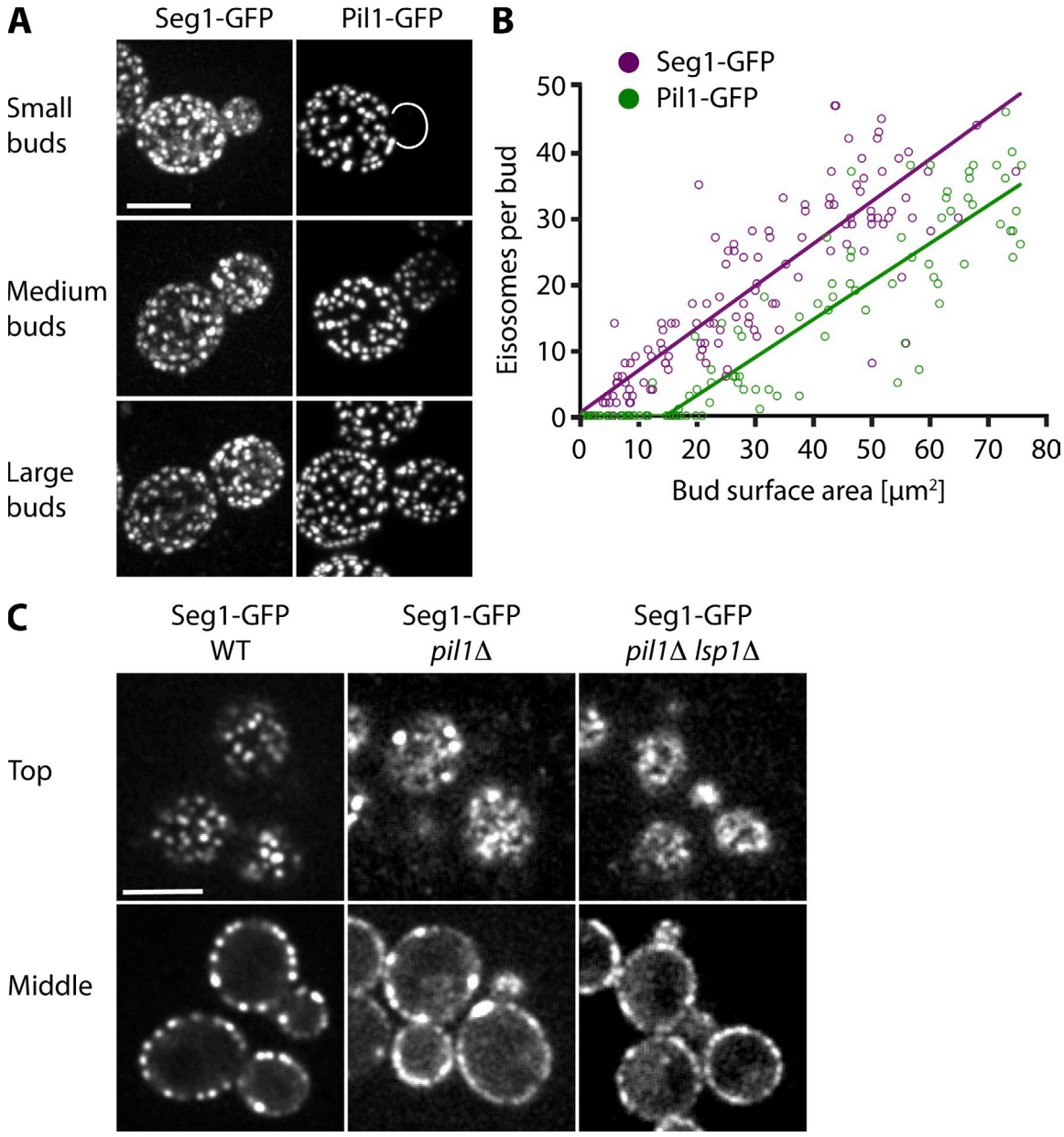

Figure 3. **Seg1 precedes Pil1 during eisosome assembly.** (A) Projections from confocal stacks of cells expressing Seg1-GFP (left) or Pil1-GFP (right). Representative images of small, medium, and large buds are shown. (B) Number of Seg1-GFP and Pil1-GFP patches per bud (determined from projections as in A), plotted against bud surface area and fitted using a biphasic model (see Materials and methods). (C) Confocal images of WT, *pil1Δ*, and *pil1Δ lsp1Δ* cells expressing Seg1-GFP. Representative top views and mid sections are shown. Bars, 5 µm.

may involve direct binding to Pil1 or Lsp1, whereas the second is independent of Pil1/Lsp1 and requires the polybasic C terminus of Seg1.

Next, we tested whether deposition of Seg1 in small buds lacking Pil1 is mediated by its C terminus. We measured the formation of Seg1Δ942-GFP patches in growing buds and found that the truncated protein was excluded from small buds almost as stringently as Pil1-GFP. Fitting of the data revealed a critical bud size for patch formation of 14 µm^2 compared with 0 µm^2 for Seg1-GFP and 15 µm^2 for Pil1-GFP (Fig. 4 E). Accordingly, the mean number of patches formed by Seg1Δ942-GFP in buds with a surface area of 1−20 µm^2 was significantly lower than that of Seg1-GFP and similar to that of Pil1-GFP (Fig. 4 F). This result shows that the C terminus is important for targeting of Seg1 to small buds. To examine the role of Seg1 targeting in eisosome assembly, we compared deposition of Pil1-GFP in buds of wild-type, *seg1Δ*, and *seg1Δ942* cells. Formation of Pil1-GFP patches in the buds of *seg1Δ* cells was diminished (Fig. 4 E). The same was true for cells expressing Seg1Δ942 as the only copy of Seg1. This result was confirmed by determining the mean number of Pil1-GFP patches in buds with a surface area of 40–75 µm^2, which revealed a reduced number of patches in *seg1Δ* and *seg1Δ942* cells (Fig. 4 G). Thus, the arrival of Seg1 in small buds by means of its lipid-binding C terminus is important for the subsequent incorporation of Pil1-GFP into nascent eisosomes.

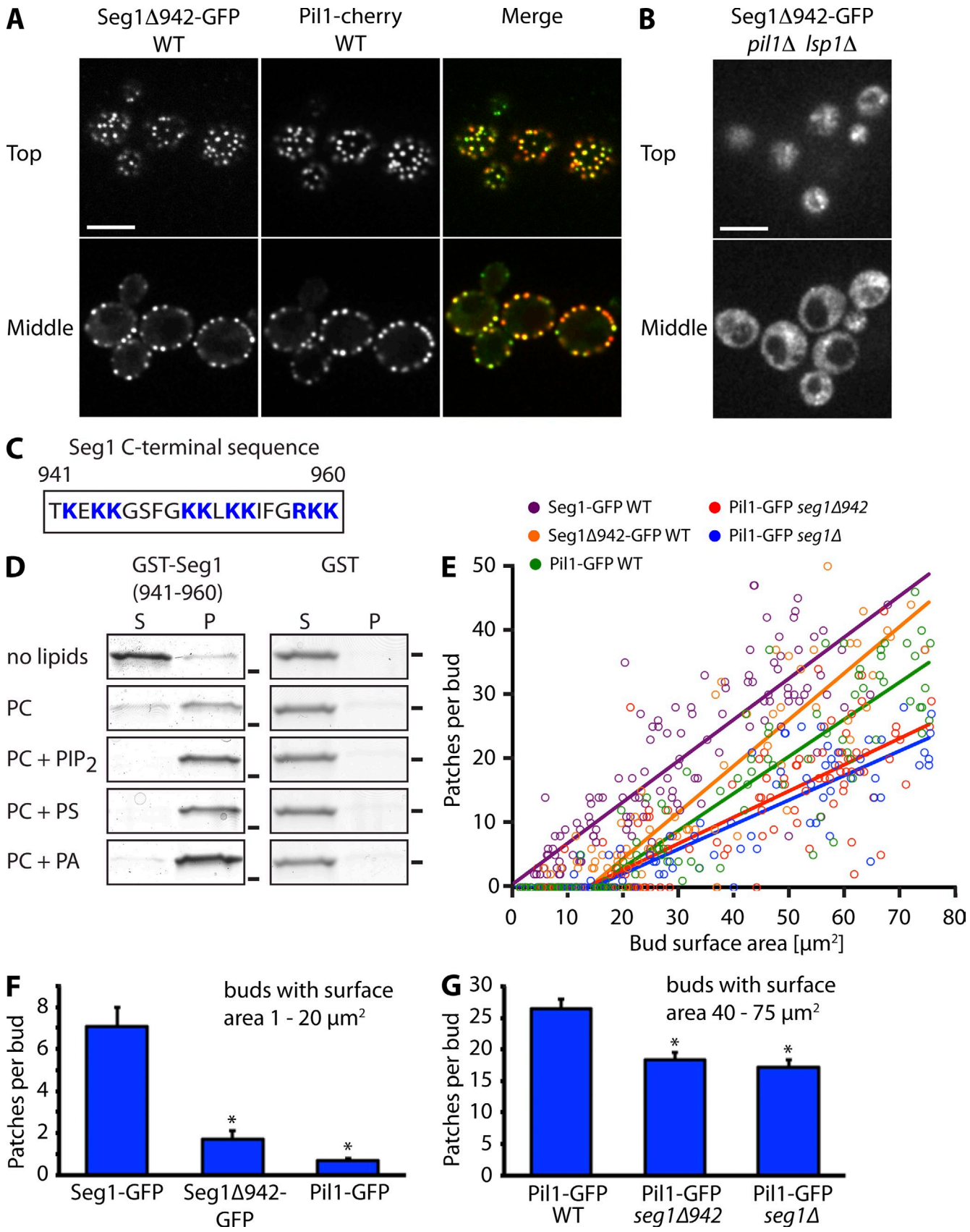

Figure 4. **Targeting of Seg1 to small buds via its lipid-binding C terminus is important for efficient eisosome assembly.** (A) Confocal images of wild-type (WT) cells expressing Seg1Δ942-GFP and Pil1-cherry. Bar, 5 µm. (B) Confocal images of *pil1Δ lsp1Δ* cells expressing Seg1Δ942-GFP. Bar, 5 µm. (C) Schematic of the C terminus of Seg1. Positively charged residues are in blue. (D) Coomassie-stained SDS-PAGE gels from spin-down assays of GST-Seg1(941–960) and GST with liposomes containing phosphatidylcholine (PC), or PC with either 1.5% PIP_2, 30% phosphatidylserine (PS), or 30%

Our results suggest the following order of events during eisosome assembly: first, the C-terminus of Seg1 mediates Pil1/Lsp1-independent targeting to the plasma membrane in small buds, where Seg1 assembles into loose patches. Pil1/Lsp1 then arrives at these patches and stabilizes them into well-defined eisosomes. Whether all Seg1 patches become eisosomes or some represent unproductive intermediates remains to be established. Because Seg1Δ942 supports a normal steady-state distribution of Pil1, Seg1 is ultimately dispensable for the targeting of Pil1/Lsp1 to the plasma membrane. Nevertheless, the early arrival of Seg1 is important for efficient eisosome assembly, perhaps by ensuring that no assembly is initiated at sites devoid of Seg1.

Seg1 controls eisosome shape

If Seg1 indeed helps organize eisosome assembly, raising Seg1 levels might change eisosome morphology. We therefore placed Seg1 under the control of the copper-inducible *CUP1* promoter and followed eisosome formation using Pil1-GFP. The *CUP1* promoter is leaky (Janke et al., 2004), and the amount of Seg1 produced even in the absence of copper was sufficient for normal eisosome formation (Fig. 5 A, left). However, after overnight growth in the presence of 100 µM $CuSO_4$ to overexpress Seg1, mother cells had striking, rod-shaped eisosomes that were aligned parallel to the plane of the membrane (Fig. 5 A, right, top cell). Young daughter cells that still shared the cytoplasm with their mothers showed reduced eisosome density yet had normal, round eisosomes (Fig. 5 A, right, bottom cell). Because the amount of Pil1-GFP is unchanged by Seg1 overexpression (Fig. S2 A), eisosome overassembly in mother cells may hamper formation of new eisosomes in daughter cells.

To test if Seg1 itself assembles into elongated structures when overproduced, we tagged Seg1 with GFP and replaced the *SEG1* promoter with the *CUP1* promoter. Because of the leakiness of the *CUP1* promoter, growth in the absence of copper yielded Seg1-GFP levels somewhat higher than those in cells expressing Seg1-GFP from the endogenous *SEG1* promoter (Fig. 5 B). Growth in medium with up to 900 µM $CuSO_4$ yielded up to 50-fold higher expression levels. Seg1-GFP in the uninduced condition showed a normal distribution (Fig. 5 C, left, compare with Fig. 2 A). However, as we raised the copper concentration, Seg1-GFP structures elongated and eventually became filamentous (Fig. 5 C, right). These results suggest that Seg1 can control the shape of eisosomes.

To further explore the properties of elongated eisosomes in cells overproducing Seg1, we generated strains that constitutively express Seg1-GFP at high levels, thus obviating the need for growth with $CuSO_4$. We deleted the endogenous *SEG1* gene and integrated a Seg1-GFP construct including the *SEG1* promoter into the *URA3* locus. The *SEG1* promoter is more active in this location, resulting in approximately ninefold higher Seg1-GFP levels compared with strains expressing Seg1-GFP from the native *SEG1* locus (Fig. S2 B). These elevated levels were sufficient to generate rod-shaped eisosomes, as is best appreciated in 2D projections from confocal stacks (Fig. 6 A, left). Next, we tested whether formation of Seg1-GFP rods requires Pil1 or Lsp1. Deleting Pil1 yielded rods that were thicker but also shorter and less abundant (Fig. 6 A, middle). The increased thickness may account for the decrease in rod length and number because sequestration of Seg1-GFP into thick rods may reduce free Seg1-GFP below the concentrations necessary to drive elongation of existing rods or assembly of new ones. Additional deletion of Lsp1 had no effect (Fig. 6 A, right). These results show that overexpressed Seg1 can assemble into plasma membrane-associated rods independently of Pil1/Lsp1. In addition, they suggest that Pil1 can shape Seg1 rods by restricting their width. This finding reinforces the notion that Pil1 and Seg1 collaborate during eisosome assembly in that Seg1 provides an early platform that is reshaped upon incorporation of Pil1.

We next asked whether Seg1-GFP rods are entirely artificial structures or likely to bear informative resemblance to native eisosomes. To this end, we first tested whether Seg1-GFP rods colocalize with other eisosome components. Consistent with the results obtained with copper-induced overexpression of untagged Seg1, Seg1-GFP rods completely reorganized the intracellular distribution of Pil1-cherry, which was now found in the same rods (Fig. 6 B). Lsp1-cherry also localized to Seg1 rods, in both otherwise wild-type and *pil1Δ* cells (Figs. 6 C and S3 A). The relocalization to Seg1 rods in wild-type cells was expected because Lsp1 binds to and therefore follows Pil1. The localization of Lsp1 to Seg1 rods in the absence of Pil1, however, was surprising. Lsp1 has so far only been found in the cytoplasm and in eisosome remnants in cells lacking Pil1 (Walther et al., 2006). The fact that overproduction of Seg1 prevents Lsp1 from becoming cytoplasmic and redirects it into Seg1 rods points to a Pil1-independent interaction of Lsp1 and Seg1. Notably, Lsp1 is unable to shape Seg1-GFP rods into long, thin filaments as Pil1 does, despite closely resembling Pil1 in structure and abundance. Finally, we analyzed the distribution of ergosterol by filipin staining and found that ergosterol patches colocalize with elongated eisosomes in Seg1-GFP–overproducing cells (Fig. 6 D). Interestingly, the localization of ergosterol to Seg1-GFP rods was abolished in *pil1Δ* cells (Fig. S3 B).

Our results show that overexpressed Seg1 forms membrane-associated rod-like structures, even in the absence of Pil1. These structures contain other eisosome components, including Pil1, Lsp1, and ergosterol. Thus, formation of Seg1 rods recapitulates aspects of normal eisosome assembly and reveals a role for Seg1 in controlling eisosome shape.

phosphatidic acid (PA). S, supernatant; P, pellet. Bars indicate the position of the 26 kD marker band. (E) Number of Seg1-GFP, Seg1Δ942-GFP, and Pil1-GFP patches per bud, plotted against bud surface area and fitted as in Fig. 3 B. The data for Seg1-GFP and Pil1-GFP from Fig. 3 B are included for reference. (F) Mean number of Seg1-GFP, Seg1Δ942-GFP, and Pil1-GFP patches in buds with a surface area of 1–20 μm^2. Error bars indicate SEM, with n = 44, 39, and 37. Asterisks indicate significant difference to Seg1-GFP ($P < 10^{-5}$). (G) Mean number of Pil1-GFP patches in buds with a surface area of 40–75 μm^2 in WT, *seg1Δ942*, and *seg1Δ* cells. Error bars indicate SEM, with n = 45, 39, and 59. Asterisks indicate significant difference to Pil1-GFP in WT cells ($P < 10^{-5}$).

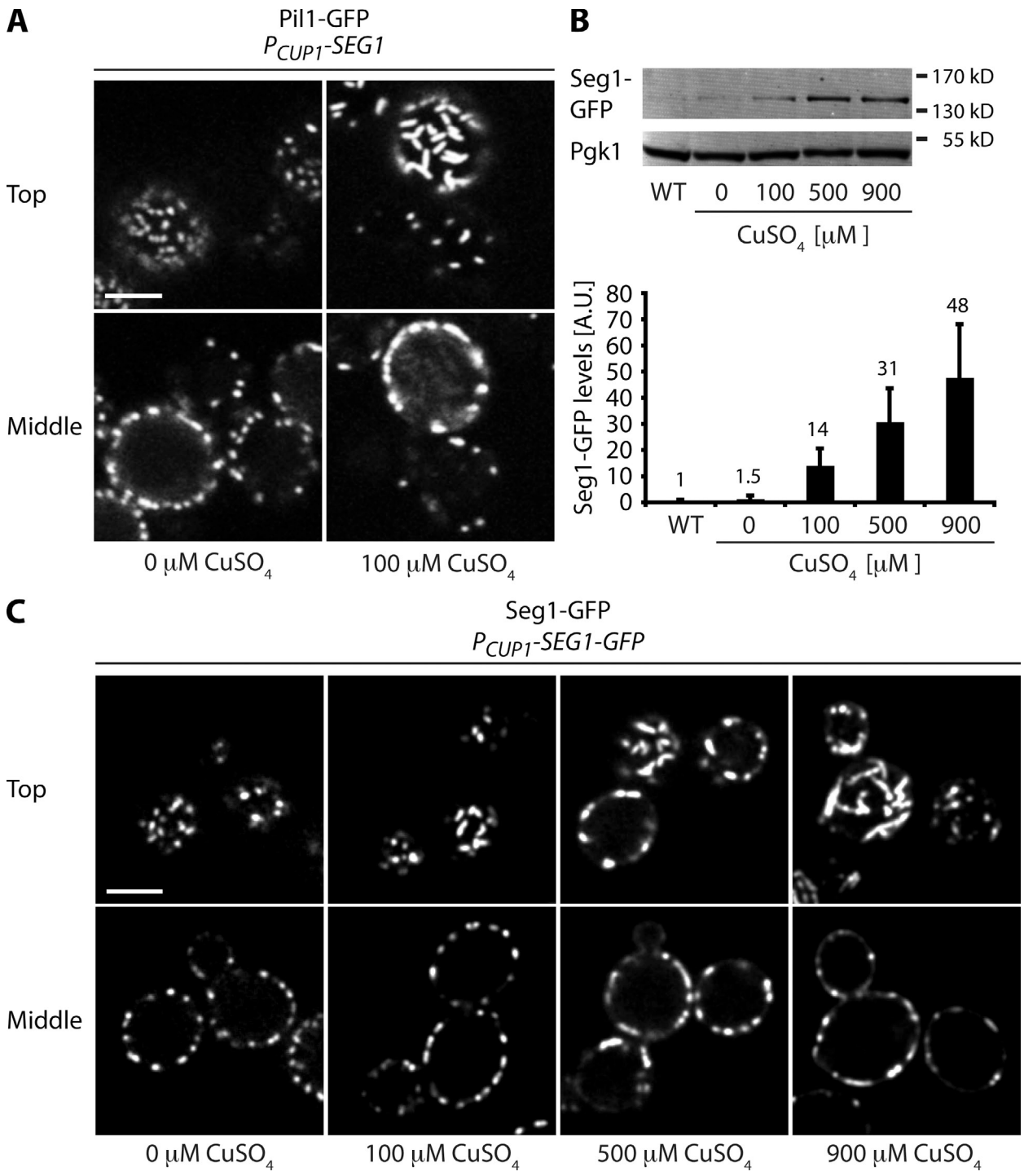

Figure 5. **Seg1 can direct the formation of rod-shaped eisosomes.** (A) Confocal images of Pil1-GFP cells expressing Seg1 from the *CUP1* promoter. Cells were grown overnight in the absence or presence of 100 µM CuSO4. (B) Western blotting and quantification of Seg1-GFP levels relative to Pgk1 in cells constitutively expressing Seg1-GFP from the *SEG1* promoter (WT) or in cells inducibly expressing Seg1-GFP from the *CUP1* promoter. The latter cells were grown overnight in the presence of 0, 100, 500, or 900 µM CuSO4. Seg1-GFP levels are in arbitrary units (A.U.). Values above the bars indicate fold change compared with WT. Error bars indicate standard deviations from three independent experiments. (C) Confocal images of cells expressing Seg1-GFP from the *CUP1* promoter grown overnight in the presence of 0, 100, 500, or 900 µM CuSO4. Representative top views and mid sections are shown. Bars, 3 µm.

Localization of Lsp1 to Seg1 rods is independent of Pil1, whereas enrichment of ergosterol at these sites requires Pil1, highlighting that Pil1 and Seg1 coordinate different steps of eisosome assembly.

Seg1 controls eisosome length

Next, we analyzed Seg1-GFP–overproducing cells by electron microscopy to determine if Seg1 rods affect plasma membrane morphology. We observed plasma membrane furrows of normal

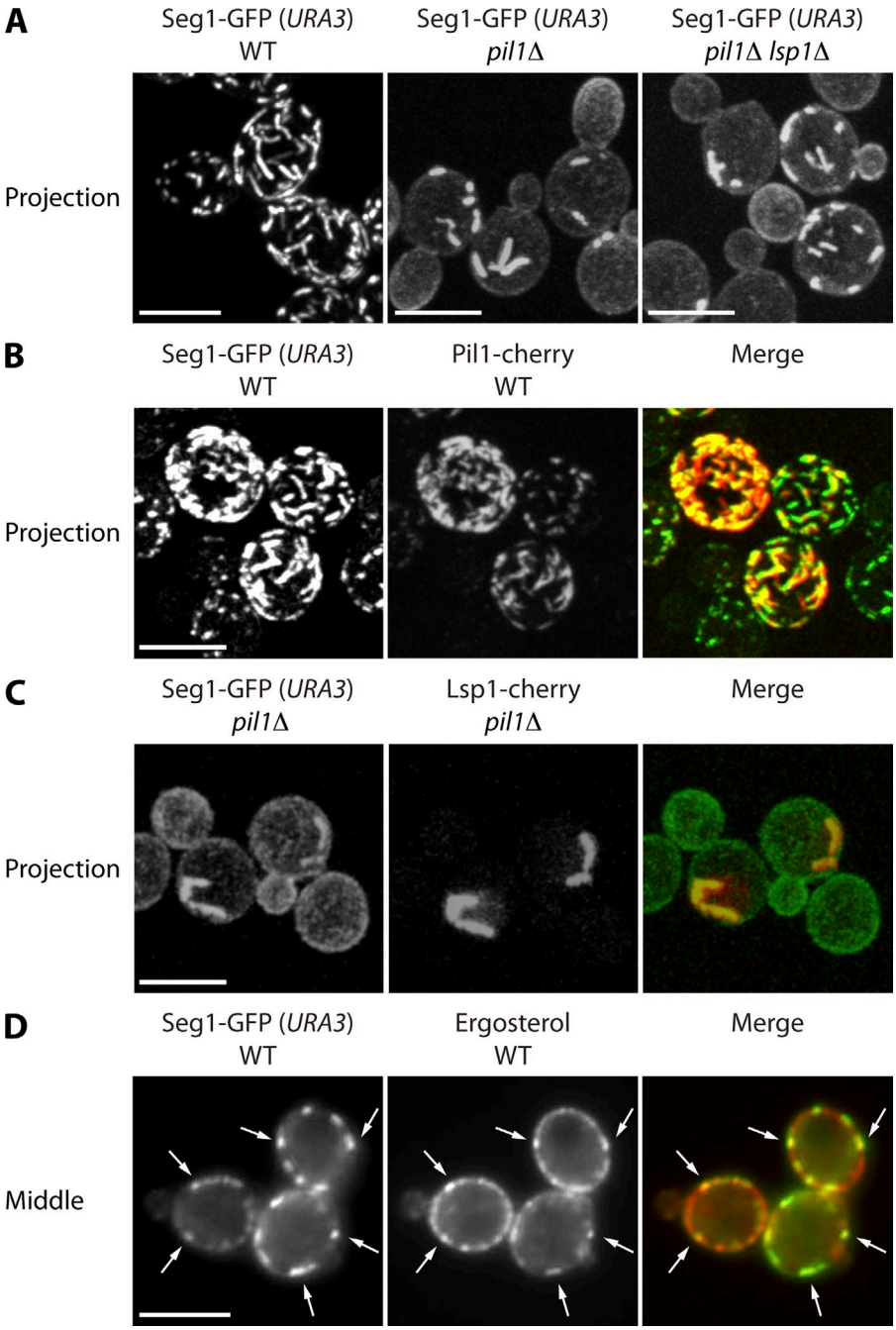

Figure 6. **Seg1 rods form without Pil1 and contain eisosome components.** (A) Projections from confocal stacks of wild-type (WT), *pil1Δ*, *and pil1Δ lsp1Δ* cells lacking endogenous Seg1 and expressing Seg1-GFP from the *URA3* locus. (B) Projections of WT cells expressing Pil1-cherry, lacking endogenous Seg1, and expressing Seg1-GFP from the *URA3* locus. (C) Projections of *pil1Δ* cells expressing Lsp1-cherry, lacking endogenous Seg1, and expressing Seg1-GFP from the *URA3* locus. (D) Epifluorescence images of WT cells lacking endogenous Seg1, expressing Seg1-GFP from the *URA3* locus, and stained with filipin to visualize ergosterol. Arrows indicate colocalization of Seg1-GFP and filipin. Bars, 5 µm.

width and depth. However, these furrows were encountered much more frequently than in cells with normal Seg1 levels (Fig. 7, A and B). Importantly, serial sections revealed that plasma membrane furrows in cells overproducing Seg1-GFP were unusually long (Fig. 8). The elongation of plasma membrane furrows likely accounts for their more frequent appearance in single thin sections because it increases the probability that furrows are captured in any given section. Quantification from serial sections showed that the furrows are 510 ± 130 nm long (n = 10), which is substantially longer than the 200 nm observed in cells with normal Seg1 levels.

To confirm that the Seg1-GFP rods seen in Seg1-overproducing cells by light microscopy and the elongated furrows observed in these cells by electron microscopy represent the same cellular structures, we used immunoelectron microscopy. We found that Seg1-GFP indeed still localized to plasma membrane invaginations (Fig. 7 C; also see Fig. S4). Grazing sections, which afford a top view of the cell surface, provided particularly clear evidence for both the elongation of plasma membrane furrows by Seg1-GFP overexpression and their specific labeling with an anti-GFP antibody (Fig. 7 D).

We also analyzed the plasma membrane morphology of *pil1Δ* cells overproducing Seg1-GFP, which display thick Seg1-GFP rods (Fig. 6). Accordingly, electron microscopy revealed large plasma membrane invaginations that were wider and much deeper than those in Seg1-GFP–overproducing wild-type cells (Fig. 7 E). Immunoelectron microscopy

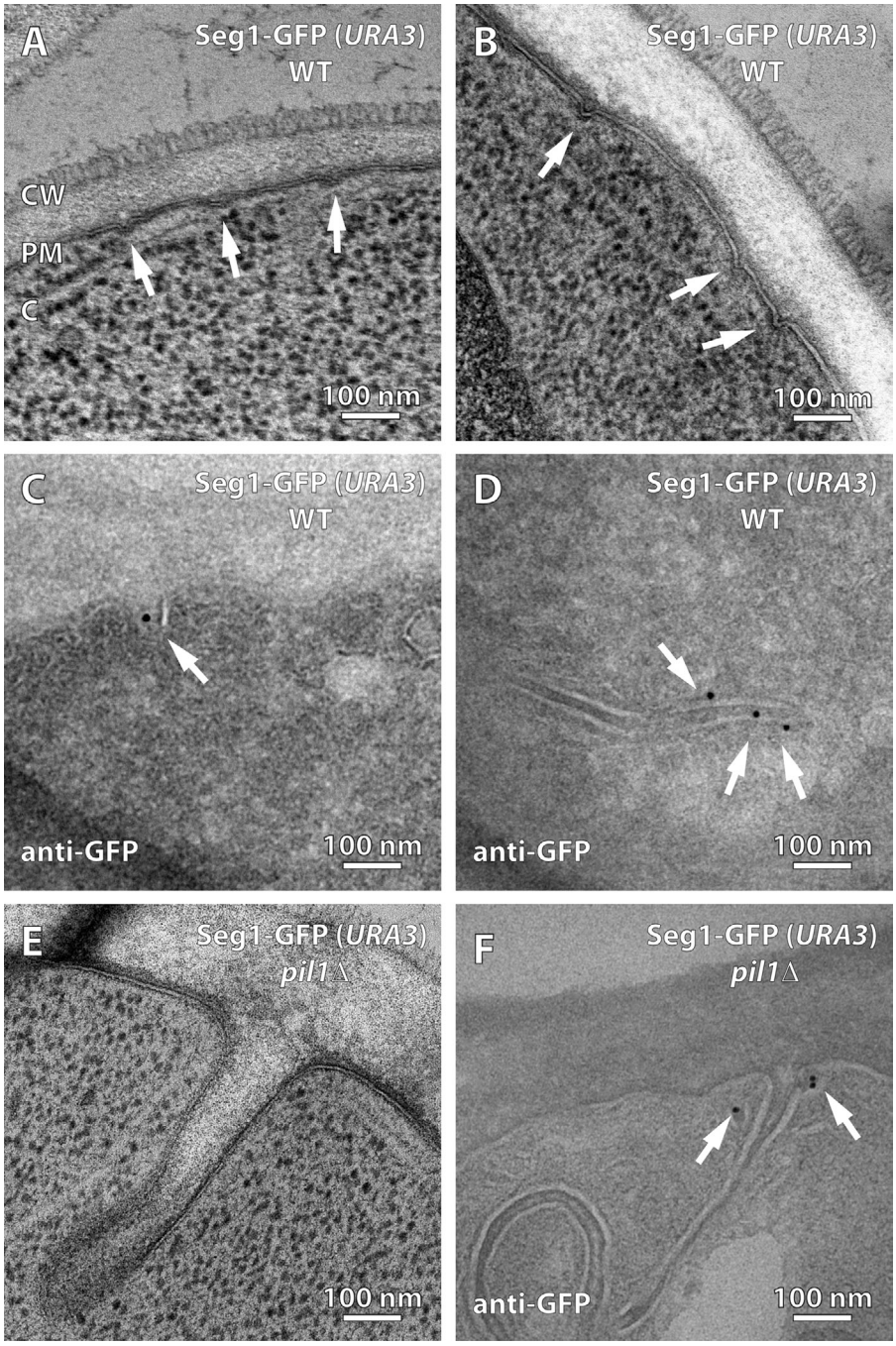

Figure 7. **Seg1 can direct the formation of plasma membrane invaginations.** (A and B) Electron micrographs of wild-type (WT) cells lacking endogenous Seg1 and expressing Seg1-GFP from the *URA3* locus. Arrows indicate plasma membrane invaginations. (C and D) Electron micrographs of the same cells labeled with anti-GFP antibody and gold-conjugated protein A. Arrows indicate gold particles. (E) Electron micrograph of *pil1Δ* cells lacking endogenous Seg1 and expressing Seg1-GFP from the *URA3* locus. (F) Electron micrograph of the same cells labeled with anti-GFP antibody and gold-conjugated protein A. Arrows indicate gold particles. CW, cell wall; PM, plasma membrane; C, cytoplasm.

confirmed that Seg1-GFP localized to these invaginations (Fig. 7 F). Intriguingly, Seg1-GFP was typically seen adjacent to the neck of these large invaginations, which may reflect a role for Seg1 in the inward bending of the plasma membrane.

In conclusion, Seg1-GFP–overproducing cells generate Seg1 rods that contain other eisosome components and shape the plasma membrane into elongated but otherwise normal furrows. These findings suggest that Seg1 rods are neither random aggregates nor eisosome remnants but true eisosomes, albeit with an altered shape. Thus, Seg1 specifically controls the geometry of eisosomes by determining their length.

Seg1-like Sle1 is required for filamentous eisosomes in *Schizosaccharomyces pombe*

The elongated eisosomes resulting from Seg1 overexpression are reminiscent of fission yeast eisosomes, which appear as elongated filaments (Kabeche et al., 2011). We therefore wondered if a Seg1-like protein in fission yeast might facilitate the assembly of elongated eisosomes in these cells. We could not identify any fission yeast gene with clear sequence homology to *S. cerevisiae SEG1*, but we examined the uncharacterized gene SPAC1A6.07 for two reasons. First, SPAC1A6.07 is a large coiled-coil protein with a polybasic C terminus (Fig. S5 A). Second, a fragment of this protein localized to eisosome-like structures in a large-scale localization study (Ding et al., 2000).

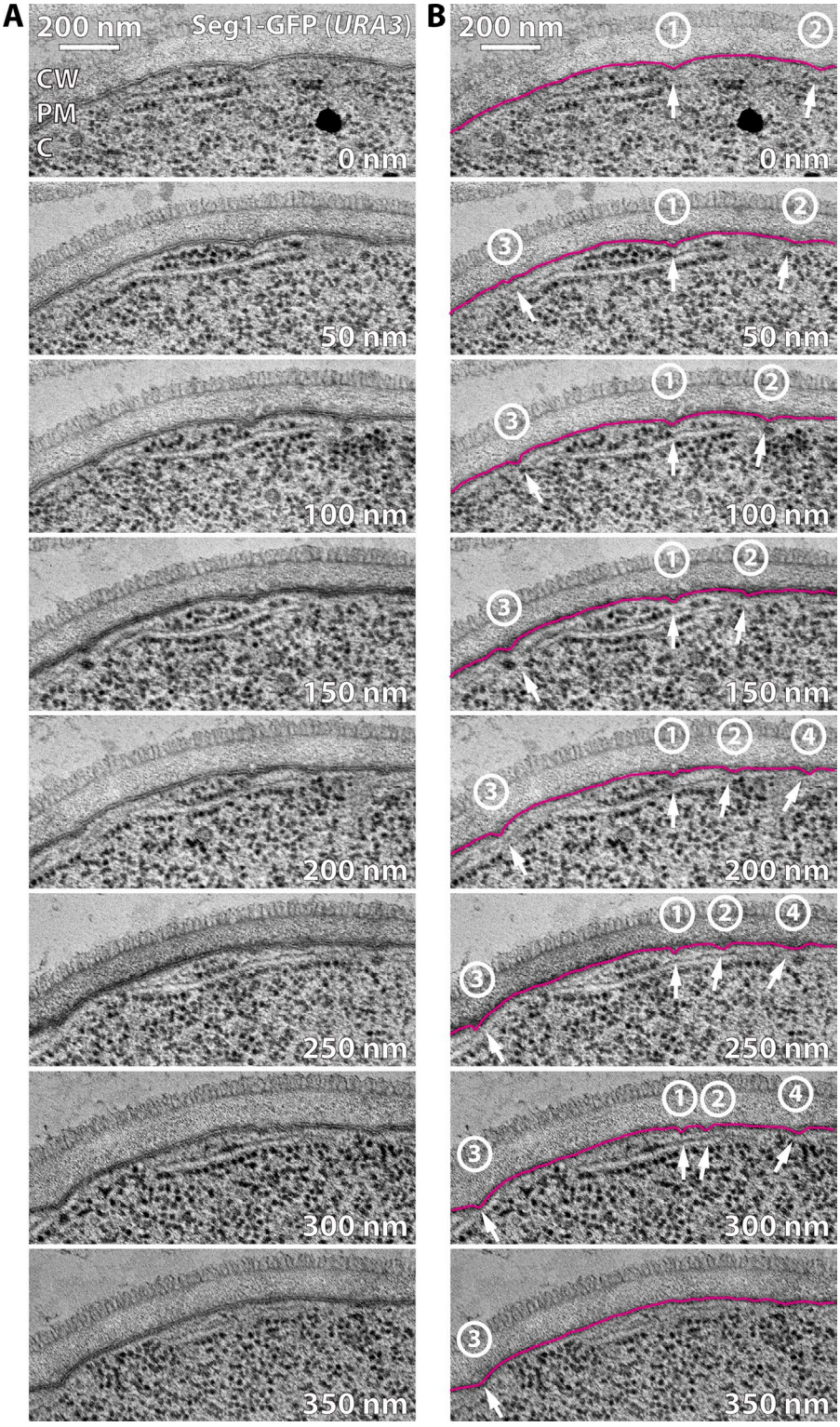

Figure 8. **Seg1 can direct the formation of long plasma membrane furrows.** (A) Electron micrographs of sequential 50-nm sections from a *seg1Δ* cell expressing Seg1-GFP from the *URA3* locus. The 200-nm image corresponds to the one shown in Fig. 6 A. CW, cell wall; PM, plasma membrane; C, cytoplasm. (B) Same micrographs as in A but the plasma membrane is traced in magenta and invaginations are indicated by arrows. Numbers denote the four furrows that can be followed in this series.

We confirmed that SPAC1A6.07 is an eisosome protein as judged by colocalization with Pil1-cherry in the middle of the cells, where mature filamentous eisosomes are found (Fig. 9 A). SPAC1A6.07 was also present at the cell tips. We mapped the eisosome-targeting domain of SPAC1A6.07 to an N-terminal region that is necessary and sufficient for colocalization with Pil1. In the absence of this region, the polybasic C terminus is required for general plasma membrane localization (Fig. S5 B). Thus, SPAC1A6.07 contains separate eisosome and plasma membrane targeting domains. Based on these similarities to *S. cerevisiae* Seg1, we have renamed this protein Sle1, for Seg1-like eisosome protein 1.

If Sle1 functions in eisosome length control in *S. pombe*, its ablation would be expected to shorten eisosomes. Indeed, Pil1-cherry filaments were disrupted in *sle1Δ* cells, showing that proper assembly of elongated eisosomes requires Sle1

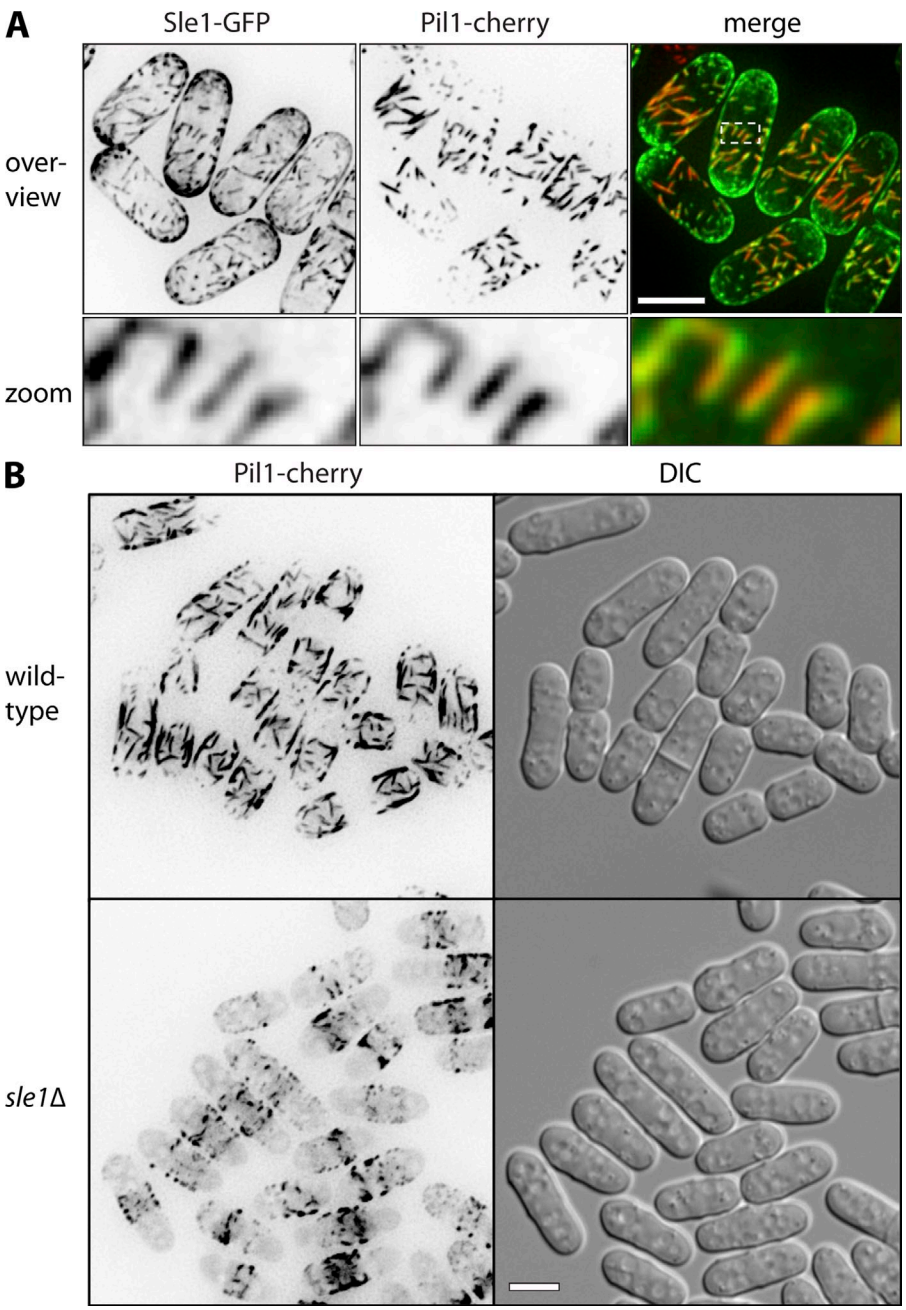

Figure 9. **Sle1/SPAC1A6.07 is an *S. pombe* eisosome protein required for filamentous eisosomes.** (A) Colocalization of Sle1 and Pil1. Images are inverted maximum projections from deconvolved z planes in the top half of cells. (B) Localization of Pil1-cherry in wild-type and *sle1Δ* cells. Images are inverted projections as in A. Bars, 5 µm.

(Fig. 9 B). Thus, Sle1 appears to function in *S. pombe* in a similar manner as Seg1 in *S. cerevisiae*, which suggests that basic features of eisosome biogenesis and architecture have been conserved between the two yeasts, despite their evolutionary divergence more than 1 billion years ago (Heckman et al., 2001).

Discussion

We have shown that Seg1 is required for proper eisosome assembly, that it precedes Pil1/Lsp1 during the formation of eisosomes, and that Seg1 levels determine eisosome length. We propose that the membrane domains generated by Seg1 serve as assembly platforms for Pil1/Lsp1, which are then converted into mature eisosomes. Hence, eisosomes arise through the coordinated assembly of mutually dependent components. Without Pil1, aberrant eisosome remnants form. Without Seg1, eisosomes assemble less efficiently and contain less Pil1. Thus, Seg1 also helps to determine the previously postulated minimum size of normal eisosomes (Moreira et al., 2009).

How could Seg1 facilitate eisosome assembly? One possibility is that Seg1 regulates Pil1 phosphorylation. Nce102 controls Pkh1/2 kinases, which can phosphorylate Pil1 on multiple sites, causing eisosome disassembly (Walther et al., 2007; Fröhlich et al., 2009). We tested the role of Seg1 in the Nce102–Pkh1/2–Pil1 phosphorylation pathway by disrupting *SEG1* in cells expressing Pil1(4A)-GFP as the only copy of Pil1. If eisosome disassembly in *seg1Δ* cells were caused by increased Pil1 phosphorylation, nonphosphorylatable Pil1(4A) eisosomes should be resistant to *SEG1* disruption. However,

Pil1(4A), like wild-type Pil1, was partially cytoplasmic in the absence of Seg1 (unpublished data). Therefore, Seg1 is not a regulator of Pil1 phosphorylation at previously identified sites. A second possibility is that Seg1 links Pil1/Lsp1 to the plasma membrane. However, cells expressing only truncated Seg1Δ942, which cannot associate with the plasma membrane without Pil1/Lsp1, show a normal steady-state distribution of Pil1 (Fig. 4 A). Therefore, Seg1 is not a tether for Pil1/Lsp1, and its C terminus is not strictly necessary for eisosome assembly. The lipid-binding C terminus does, however, ensure the early presence of Seg1 at sites of eisosome formation and makes the generation of eisosomes more efficient, possibly by restraining aberrant assembly without the participation of Seg1. A third possibility is that Seg1 remodels the plasma membrane to assist eisosome assembly. The elongated furrows produced by overexpressed Seg1 suggest that Seg1 can induce membrane bending. Pil1/Lsp1 alone are able to bind and tubulate liposomes in vitro (Karotki et al., 2011), but the generation of membrane furrows in vivo may involve additional proteins. An attractive speculation is that Seg1 initiates plasma membrane invagination and in this way prepares the deposition of Pil1/Lsp1. The subsequent assembly of the Pil1/Lsp1 lattice, which forms a half cylinder (Karotki et al., 2011), would exert a constricting force and give the membrane its final shape. Without prior membrane remodeling by Seg1, Pil1/Lsp1 may produce less stable eisosomes, resulting in the observed partial localization of Pil1 to the cytoplasm. This scenario is consistent with work on the *A. gossypii* Seg1, which is dispensable for the initial targeting of Pil1 to regions of eisosome formation but required for its sustained membrane association (Seger et al., 2011). How Seg1 specifically controls eisosome length remains to be discovered but may involve Seg1 polymers that serve as a ruler. Furthermore, there must be additional morphogenic factors because irregularly shaped plasma membrane invaginations persist in a quadruple mutant lacking Pil1, Lsp1, Seg1, and Seg2 (unpublished data).

The yeast gene most closely related to *SEG1* is *SEG2/YKL105C*. Like *SEG1*, *SEG2* encodes a large coiled-coil protein with a polybasic C terminus. The Seg2 protein directly or indirectly interacts with Seg1 (Fig. 2 D). Similar to Seg1-GFP, Seg2-GFP localizes to eisosomes and requires the basic C terminus of Seg2 for plasma membrane association in the absence of Pil1/Lsp1 (unpublished data). Nevertheless, we found that disruption of *SEG2* does not impair eisosome assembly and only slightly exacerbates the *seg1* mutant phenotype. Furthermore, Seg2 protein levels are 10-fold lower than those of Seg1, or 100-fold lower than those of Pil1. Thus, Seg2 is an eisosome component but likely plays only a minor role in eisosome assembly.

Our study extends the intriguing similarities between eisosomes and caveolae. Until recently, the caveolins (caveolin-1/2/3) were thought to be the sole structural proteins of caveolae. Caveolins assume hairpin structures in the membrane, assemble into large protein lattices, and shape cholesterol/sphingolipid-rich membranes into cuplike caveolae by wedging and scaffolding (Shibata et al., 2009). This picture has become more complex with the discovery of the cavins (cavin-1/2/3/4; Hansen and Nichols, 2010). Cavins are cytosolic coiled-coil proteins that form large complexes with one another, contain polybasic regions, and bind phosphatidylserine (Burgener et al., 1990; Hill et al., 2008; Bastiani et al., 2009). Interestingly, caveolins cluster phosphatidylserine (Wanaski et al., 2003) and may thereby create multivalent binding platforms for the cavins. Depleting or removing cavin-1 or cavin-2 causes loss of caveolae (Hill et al., 2008; Liu et al., 2008; Hansen et al., 2009; McMahon et al., 2009). In the absence of cavin-1, caveolin-1 diffuses in the plasma membrane, indicating that cavins immobilize caveolins at invaginated caveolar membranes (Hill et al., 2008). Cavin-2 overexpression induces long plasma membrane tubules (Hansen et al., 2009). Caveolin-1 overexpression also causes tubule formation, which can be suppressed by raising cavin-1 levels (Verma et al., 2010). Thus, proper caveola morphology depends on the balance between caveolins and cavins. During caveola biogenesis, caveolin complexes arrive at the plasma membrane first, where they organize domains rich in cholesterol, sphingolipids, and possibly phosphatidylserine. Incipient caveolae are then stabilized by cavin complexes (Hayer et al., 2010). Finally, Pacsin 2, a BAR domain protein, has recently been found to participate in caveola biogenesis (Hansen et al., 2011; Senju et al., 2011).

These new findings reveal principles of construction that are shared by caveolae and eisosomes. Both domains consist of characteristic plasma membrane invaginations coated with heteromultimeric protein scaffolds. Both caveolae and eisosomes self-assemble in a stepwise fashion, with caveolins and Seg1 arriving first, followed by cavins and Pil1/Lsp1. Generation of the proper plasma membrane shape requires balanced levels of mutually dependent components in both cases, as is evident from the contorted morphologies produced by overexpression of cavin-2, caveolin-1, or Seg1. In addition, caveolar and eisosome shape generation involves BAR domain proteins, namely Pacsin 2 and Pil1/Lsp1. Finally, both caveolae and eisosomes are domains rich in sterols and sphingolipids and may use negatively charged lipids, such as phosphatidylserine and phosphatidylinositol-4,5-bisphosphate (Fujita et al., 2009), for the recruitment of some of their protein components, including cavins and Seg1. Caveolae and eisosomes therefore represent a remarkable example of convergent evolution, in which unrelated proteins assemble into corresponding structures by means of strikingly similar architectural principles.

How the form of eisosomes relates to their functions remains to be resolved. Paradoxically, eisosomes have been proposed to act as endocytic portals similar to caveolae (Walther et al., 2006), to constitute membrane domains protected from endocytosis (Grossmann et al., 2008), and to have no role in endocytosis at all (Brach et al., 2011). The elongated and easily visible eisosomes generated by Seg1 overexpression may prove useful in investigating the controversial spatial organization of yeast endocytosis. We anticipate that our still limited understanding of eisosome function will improve rapidly as we elaborate new ways of manipulating eisosome architecture.

Materials and methods

S. cerevisiae strains

Strains used in this study are listed in Table S1. Most chromosomal integrations and replacements were introduced by homologous recombination using PCR products (Longtine et al., 1998; Janke et al., 2004). To generate strains expressing Seg1-GFP from the *URA3* locus, the *SEG1-GFP* coding sequence including 536 upstream base pairs was PCR-amplified from strain KEM130 and cloned between the SacI and HindIII sites of pRS306 (Sikorski and Hieter, 1989). The resulting vector pRS306-Seg1-GFP was integrated into the *URA3* gene.

S. cerevisiae culture

Strains were cultured at 30°C in complete synthetic (SC) medium with 2% dextrose. For labeling with light and heavy lysine, cells were grown overnight for at least 10 doubling times in 100 ml of SC medium containing 30 mg/liter normal L-lysine or L-lysine-U-$^{13}C_6$, $^{15}N_2$, respectively, until cultures had reached OD_{600} = 0.7. For induction of copper-controlled expression, strains were grown to early log phase (OD_{600} = 0.2–0.3) and diluted into medium containing up to 900 µM $CuSO_4$ such that they reached early log phase again after overnight culture.

Western blotting

Strains were grown to mid log phase (OD_{600} = 0.5); cell lysates were prepared in 8 M urea, 2% SDS, and 50 mM Hepes, pH 7.4; and protein concentrations were determined by bicinchoninic acid protein assay (Thermo Fisher Scientific). Equal amounts of protein were resolved by SDS-PAGE and transferred onto polyvinylidene difluoride membranes. GFP fusion proteins were detected with mouse anti-GFP antibody 7.1/13.1 (Roche). Pgk1 was detected with mouse anti-Pgk1 antibody 22C5 (Invitrogen). After incubation with primary antibodies, membranes were probed with alkaline phosphatase–conjugated secondary antibodies (EMD Millipore) and incubated with enhanced chemifluorescence substrate (GE Healthcare). Fluorescence was detected and bands were quantified with a Typhoon 9400 variable mode imager equipped with Image Quant software (GE Healthcare).

Proteomics

Protein extraction, affinity purification, sample processing, and mass spectrometry were performed as described previously (Aguilar et al., 2010). In brief, equivalent amounts of protein from wild-type cells (strain TWY70) labeled with normal light L-lysine and Seg1-TEV-GFP cells (strain TWY1118) labeled with heavy L-lysine-U-$^{13}C_6$, $^{15}N_2$ were incubated with anti-GFP antibody conjugated to magnetic nanobeads (Miltenyi Biotech). Bound proteins were eluted by tobacco etch virus (TEV) protease cleavage. Eluates from the two strains were mixed, reduced, alkylated, and digested with endoproteinase LysC. The resulting peptide mixtures were separated by HPLC and analyzed using an LTQ-Orbitrap Velos mass spectrometer (Thermo Fisher Scientific).

Light microscopy

Strains were grown to mid-log phase and cells were mounted onto coverslips coated with Concanavalin A. Images were taken at room temperature on a laser-scanning confocal microscope (LSM510; Carl Zeiss) and an inverted microscope (TE2000U; Nikon) with a Yokogawa CSU22 spinning disk confocal from Solamere Technology (provided by the Nikon Imaging Center, University of California, San Francisco, CA), controlled by Micro-manager (Edelstein et al., 2010), or a Deltavision Imaging System (Applied Precision; Kabeche et al., 2011). Images were processed using ImageJ software. Cytoplasmic and eisosomal Pil1-GFP fluorescence were quantified according to Fröhlich et al. (2009). Bud surface areas were quantified from confocal stacks according to Moreira et al. (2009). Buds were treated as spheroids, and bright field images capturing the middle of a bud were used to measure bud length (the distance from bud neck to bud tip) and width. Surface area was calculated using $S = 2\pi a^2 + 2\pi(ab/e)\sin^{-1} e$, where a is bud length, b is bud width, and $e = [\sqrt{}]1 - (b^2/a^2)$. The number of GFP patches per bud was determined from 3D reconstructions generated from fluorescent images from the same confocal stacks. The number of patches was plotted against bud surface area and data were fitted using a biphasic model that assumes a lag phase followed by a linear increase of patch number with bud size. The two fitted parameters were the critical bud size for patch formation, which marks the end of the lag phase, and the slope of the subsequent increase. To visualize ergosterol, cells were washed with 50 mM potassium phosphate, pH 5.5, stained with 2 µg/ml filipin (Sigma-Aldrich) for 5 min, washed again, and imaged at room temperature with a wide-field microscope (Axiovert 200M; Carl Zeiss).

Electron microscopy

For regular electron microscopy, strains were grown to early log phase in yeast extract peptone dextrose (YPD) medium containing 1% dextrose. Cells were processed as described previously (Schuck et al., 2009). In brief, cells were harvested by filtration, rapidly frozen using an EM PACT high-pressure freezer (Leica), freeze substituted in fixative (1% osmium tetroxide, 0.1% uranyl acetate, and 3% water in acetone) using an EM AFS2 freeze substitution system (Leica), and embedded in epon resin. 50–90-nm-thin sections were cut, stained with uranyl acetate and Reynold's lead citrate, and viewed with a transmission electron microscope (Tecnai 12; FEI). For immunoelectron microscopy, strains were grown to mid-log phase in YPD medium containing 2% dextrose, concentrated by filtration, chemically fixed, treated with periodic acid, embedded in gelatin, and infused with sucrose according to Griffith et al. (2008). Blocks were frozen in liquid nitrogen, and 75-nm-thin cryo-sections were cut with a cryo-ultramicrotome (Ultracut UCT with EM FCS; Leica) at −110°C and placed on Formvar-coated nickel grids. For immunolabeling, sections were incubated with polyclonal rabbit anti-GFP antibodies (Abcam), followed by incubation with protein A-10 nm gold (CMC, Universitair Medisch Centrum Utrecht). After contrasting with 0.4% (wt/vol) uranyl acetate in 2 M methyl-cellulose and embedding in the same solution, sections were examined with a transmission electron microscope (CM120; Philips).

Liposome binding assay

The 20 C-terminal amino acids of Seg1 were cloned into pGEX-pP-2 (GE Healthcare). The resulting GST-Seg1(941–960) fusion protein was expressed in *E. coli* strain BL21DE3RIPL by IPTG induction, purified over a glutathione-Sepharose column in buffer A (150 mM sodium chloride, 50 mM Tris, pH 7.6, 2.5% glycerol, 3 mM β-mercaptoethanol, and 1 mM PMSF) and concentrated on a S200 Superdex column (GE Healthcare). Lipids (Avanti Polar Lipids, Inc.) were mixed (pure phosphatidylcholine, or phosphatidylcholine with 1.5% PIP_2, 30% phosphatidylserine, or 30% phosphatidic acid), dried under an argon stream, dissolved in buffer A at 9 mM, subjected to five freeze–thaw cycles, and extruded at 65°C through a 200-nm pore-size polycarbonate filter using a mini extruder (Avanti Polar Lipids, Inc.). GST-Seg1(941–960) or GST (Sigma-Aldrich) at 3 µM were incubated in the presence or absence of 4 mM liposomes in 40 µl buffer A at room temperature for 20 min. Samples were centrifuged with an OptimaTXL ultracentrifuge (Beckman) using a TLA.100 rotor at 47,000 rpm at 4°C for 30 min. Supernatants and pellets were collected, adjusted to equal volumes, and analyzed by SDS-PAGE and Coomassie blue staining.

S. pombe strains and techniques

Standard *S. pombe* media and methods were used (Moreno et al., 1991). Gene tagging and deletion were performed using PCR and homologous recombination (Bähler et al., 1998). Strains JM1262 (*pil1-cherry::NAT^R h−*) and JM1467 (*sle1Δ::KAN^R pil1-cherry::NAT^R leu1-32*) were used in this study. For localization of Sle1 constructs, the coding sequence was subcloned into pREP41 containing a C-terminal GFP tag, and the resulting plasmids were transformed into strain JM1467. Expression was induced by growth in minimal medium lacking thiamine for 20 h before imaging.

Online supplemental material

Fig. S1 shows electron micrographs of serial thin sections of wild-type and *seg1Δ* cells. Fig. S2 shows Pil1-GFP and Seg1-GFP levels in Seg1-overexpression strains. Fig. S3 shows localization of Lsp1-cherry and ergosterol to Seg1-GFP rods. Fig. S4 shows immunogold labeling of GFP in cells overexpressing Seg1-GFP. Fig. S5 shows domain analysis of *S. pombe* Sle1. Table S1 list the *S. cerevisiae* strains used in this study. Online supplemental material is available at http://www.jcb.org/cgi/content/full/jcb.201202097/DC1.

We thank Mei-Lie Wong and Jon Mulholland for help with electron microscopy, Kurt Thorn at the Nikon Imaging Center at University of California, San Francisco, for help with light microscopy, Matthias Mann for providing the instruments for mass spectrometric analysis, Katja Gotthard for help with protein purification, Lena Karotki for help with spin-down assays, and Martin Kampmann and Hana El-Samad for help with curve fitting. We are grateful to Blanche Schwappach for support and to Dietmar Riedel and Dirk Wenzel at the Max Planck for Biophysical Chemistry Göttingen for providing the equipment for immuno-EM.

S. Schuck was supported by a postdoctoral fellowship from the Human Frontier Science Program. T.C. Walther and F. Fröhlich acknowledge support from the German Research Council (DFG) and the Minna-James-Heineman

Foundation. J.B. Moseley is supported by grants from the National Institutes of Health (P30GM092357) and the American Cancer Society (#IRG-82-003-26), and is a Pew Scholar in the Biomedical Sciences. This work was supported by grants to P. Walter from the National Institutes of Health (R01GM32384). P. Walter is an Investigator of the Howard Hughes Medical Institute.

Submitted: 17 February 2012
Accepted: 5 July 2012

References

Aguilar, P.S., F. Fröhlich, M. Rehman, M. Shales, I. Ulitsky, A. Olivera-Couto, H. Braberg, R. Shamir, P. Walter, M. Mann, et al. 2010. A plasma-membrane E-MAP reveals links of the eisosome with sphingolipid metabolism and endosomal trafficking. *Nat. Struct. Mol. Biol.* 17:901–908. http://dx.doi.org/10.1038/nsmb.1829

Bähler, J., J.Q. Wu, M.S. Longtine, N.G. Shah, A. McKenzie III, A.B. Steever, A. Wach, P. Philippsen, and J.R. Pringle. 1998. Heterologous modules for efficient and versatile PCR-based gene targeting in *Schizosaccharomyces pombe. Yeast*. 14:943–951. http://dx.doi.org/10.1002/(SICI)1097-0061(199807)14:10<943::AID-YEA292>3.0.CO;2-Y

Bastiani, M., and R.G. Parton. 2010. Caveolae at a glance. *J. Cell Sci.* 123:3831–3836. http://dx.doi.org/10.1242/jcs.070102

Bastiani, M., L. Liu, M.M. Hill, M.P. Jedrychowski, S.J. Nixon, H.P. Lo, D. Abankwa, R. Luetterforst, M. Fernandez-Rojo, M.R. Breen, et al. 2009. MURC/Cavin-4 and cavin family members form tissue-specific caveolar complexes. *J. Cell Biol.* 185:1259–1273. http://dx.doi.org/10.1083/jcb.200903053

Brach, T., T. Specht, and M. Kaksonen. 2011. Reassessment of the role of plasma membrane domains in the regulation of vesicular traffic in yeast. *J. Cell Sci.* 124:328–337. http://dx.doi.org/10.1242/jcs.078519

Burgener, R., M. Wolf, T. Ganz, and M. Baggiolini. 1990. Purification and characterization of a major phosphatidylserine-binding phosphoprotein from human platelets. *Biochem. J.* 269:729–734.

Caudron, F., and Y. Barral. 2009. Septins and the lateral compartmentalization of eukaryotic membranes. *Dev. Cell*. 16:493–506. http://dx.doi.org/10.1016/j.devcel.2009.04.003

Deng, C., X. Xiong, and A.N. Krutchinsky. 2009. Unifying fluorescence microscopy and mass spectrometry for studying protein complexes in cells. *Mol. Cell. Proteomics*. 8:1413–1423. http://dx.doi.org/10.1074/mcp.M800397-MCP200

Ding, D.Q., Y. Tomita, A. Yamamoto, Y. Chikashige, T. Haraguchi, and Y. Hiraoka. 2000. Large-scale screening of intracellular protein localization in living fission yeast cells by the use of a GFP-fusion genomic DNA library. *Genes Cells*. 5:169–190. http://dx.doi.org/10.1046/j.1365-2443.2000.00317.x

Edelstein, A., N. Amodaj, K. Hoover, R. Vale, and N. Stuurman. 2010. Computer control of microscopes using μManager. *Curr. Protoc. Mol. Biol.* Chapter 14:Unit 14.20. http://dx.doi.org/10.1002/0471142727.mb1420s92

Fröhlich, F., K. Moreira, P.S. Aguilar, N.C. Hubner, M. Mann, P. Walter, and T.C. Walther. 2009. A genome-wide screen for genes affecting eisosomes reveals Nce102 function in sphingolipid signaling. *J. Cell Biol.* 185:1227–1242. http://dx.doi.org/10.1083/jcb.200811081

Fujita, A., J. Cheng, K. Tauchi-Sato, T. Takenawa, and T. Fujimoto. 2009. A distinct pool of phosphatidylinositol 4,5-bisphosphate in caveolae revealed by a nanoscale labeling technique. *Proc. Natl. Acad. Sci. USA*. 106:9256–9261. http://dx.doi.org/10.1073/pnas.0900216106

Ghaemmaghami, S., W.K. Huh, K. Bower, R.W. Howson, A. Belle, N. Dephoure, E.K. O'Shea, and J.S. Weissman. 2003. Global analysis of protein expression in yeast. *Nature*. 425:737–741. http://dx.doi.org/10.1038/nature02046

Griffith, J., M. Mari, A. De Mazière, and F. Reggiori. 2008. A cryosectioning procedure for the ultrastructural analysis and the immunogold labelling of yeast *Saccharomyces cerevisiae. Traffic*. 9:1060–1072. http://dx.doi.org/10.1111/j.1600-0854.2008.00753.x

Grossmann, G., M. Opekarová, L. Novakova, J. Stolz, and W. Tanner. 2006. Lipid raft-based membrane compartmentation of a plant transport protein expressed in *Saccharomyces cerevisiae. Eukaryot. Cell*. 5:945–953. http://dx.doi.org/10.1128/EC.00206-05

Grossmann, G., M. Opekarová, J. Malínsky, I. Weig-Meckl, and W. Tanner. 2007. Membrane potential governs lateral segregation of plasma membrane proteins and lipids in yeast. *EMBO J.* 26:1–8. http://dx.doi.org/10.1038/sj.emboj.7601466

Grossmann, G., J. Malínsky, W. Stahlschmidt, M. Loibl, I. Weig-Meckl, W.B. Frommer, M. Opekarová, and W. Tanner. 2008. Plasma membrane microdomains regulate turnover of transport proteins in yeast. *J. Cell Biol.* 183:1075–1088. http://dx.doi.org/10.1083/jcb.200806035

Hansen, C.G., and B.J. Nichols. 2009. Molecular mechanisms of clathrin-independent endocytosis. *J. Cell Sci.* 122:1713–1721. http://dx.doi.org/10.1242/jcs.033951

Hansen, C.G., and B.J. Nichols. 2010. Exploring the caves: cavins, caveolins and caveolae. *Trends Cell Biol.* 20:177–186. http://dx.doi.org/10.1016/j.tcb.2010.01.005

Hansen, C.G., N.A. Bright, G. Howard, and B.J. Nichols. 2009. SDPR induces membrane curvature and functions in the formation of caveolae. *Nat. Cell Biol.* 11:807–814. http://dx.doi.org/10.1038/ncb1887

Hansen, C.G., G. Howard, and B.J. Nichols. 2011. Pacsin 2 is recruited to caveolae and functions in caveolar biogenesis. *J. Cell Sci.* 124:2777–2785. http://dx.doi.org/10.1242/jcs.084319

Hayer, A., M. Stoeber, C. Bissig, and A. Helenius. 2010. Biogenesis of caveolae: stepwise assembly of large caveolin and cavin complexes. *Traffic*. 11:361–382. http://dx.doi.org/10.1111/j.1600-0854.2009.01023.x

Heckman, D.S., D.M. Geiser, B.R. Eidell, R.L. Stauffer, N.L. Kardos, and S.B. Hedges. 2001. Molecular evidence for the early colonization of land by fungi and plants. *Science*. 293:1129–1133. http://dx.doi.org/10.1126/science.1061457

Hill, M.M., M. Bastiani, R. Luetterforst, M. Kirkham, A. Kirkham, S.J. Nixon, P. Walser, D. Abankwa, V.M. Oorschot, S. Martin, et al. 2008. PTRF-Cavin, a conserved cytoplasmic protein required for caveola formation and function. *Cell*. 132:113–124. http://dx.doi.org/10.1016/j.cell.2007.11.042

Janke, C., M.M. Magiera, N. Rathfelder, C. Taxis, S. Reber, H. Maekawa, A. Moreno-Borchart, G. Doenges, E. Schwob, E. Schiebel, and M. Knop. 2004. A versatile toolbox for PCR-based tagging of yeast genes: new fluorescent proteins, more markers and promoter substitution cassettes. *Yeast*. 21:947–962. http://dx.doi.org/10.1002/yea.1142

Kabeche, R., S. Baldissard, J. Hammond, L. Howard, and J.B. Moseley. 2011. The filament-forming protein Pil1 assembles linear eisosomes in fission yeast. *Mol. Biol. Cell*. 22:4059–4067. http://dx.doi.org/10.1091/mbc.E11-07-0605

Karotki, L., J.T. Huiskonen, C.J. Stefan, N.E. Ziółkowska, R. Roth, M.A. Surma, N.J. Krogan, S.D. Emr, J. Heuser, K. Grünewald, and T.C. Walther. 2011. Eisosome proteins assemble into a membrane scaffold. *J. Cell Biol.* 195:889–902. http://dx.doi.org/10.1083/jcb.201104040

Lingwood, D., and K. Simons. 2010. Lipid rafts as a membrane-organizing principle. *Science*. 327:46–50. http://dx.doi.org/10.1126/science.1174621

Liu, L., D. Brown, M. McKee, N.K. Lebrasseur, D. Yang, K.H. Albrecht, K. Ravid, and P.F. Pilch. 2008. Deletion of Cavin/PTRF causes global loss of caveolae, dyslipidemia, and glucose intolerance. *Cell Metab.* 8:310–317. http://dx.doi.org/10.1016/j.cmet.2008.07.008

Longtine, M.S., A. McKenzie III, D.J. Demarini, N.G. Shah, A. Wach, A. Brachat, P. Philippsen, and J.R. Pringle. 1998. Additional modules for versatile and economical PCR-based gene deletion and modification in *Saccharomyces cerevisiae. Yeast*. 14:953–961. http://dx.doi.org/10.1002/(SICI)1097-0061(199807)14:10<953::AID-YEA293>3.0.CO;2-U

Luo, G., A. Gruhler, Y. Liu, O.N. Jensen, and R.C. Dickson. 2008. The sphingolipid long-chain base-Pkh1/2-Ypk1/2 signaling pathway regulates eisosome assembly and turnover. *J. Biol. Chem.* 283:10433–10444. http://dx.doi.org/10.1074/jbc.M709972200

Malínská, K., J. Malínský, M. Opekarová, and W. Tanner. 2003. Visualization of protein compartmentation within the plasma membrane of living yeast cells. *Mol. Biol. Cell*. 14:4427–4436. http://dx.doi.org/10.1091/mbc.E03-04-0221

Malínská, K., J. Malínsky, M. Opekarová, and W. Tanner. 2004. Distribution of Can1p into stable domains reflects lateral protein segregation within the plasma membrane of living *S. cerevisiae* cells. *J. Cell Sci.* 117:6031–6041. http://dx.doi.org/10.1242/jcs.01493

Malínsky, J., M. Opekarová, and W. Tanner. 2010. The lateral compartmentation of the yeast plasma membrane. *Yeast*. 27:473–478. http://dx.doi.org/10.1002/yea.1772

McMahon, K.A., H. Zajicek, W.P. Li, M.J. Peyton, J.D. Minna, V.J. Hernandez, K. Luby-Phelps, and R.G. Anderson. 2009. SRBC/cavin-3 is a caveolin adapter protein that regulates caveolae function. *EMBO J.* 28:1001–1015. http://dx.doi.org/10.1038/emboj.2009.46

Moor, H., and K. Mühlethaler. 1963. Fine structure of frozen-etched yeast cells. *J. Cell Biol.* 17:609–628. http://dx.doi.org/10.1083/jcb.17.3.609

Moreira, K.E., T.C. Walther, P.S. Aguilar, and P. Walter. 2009. Pil1 controls eisosome biogenesis. *Mol. Biol. Cell*. 20:809–818. http://dx.doi.org/10.1091/mbc.E08-03-0313

Moreno, S., A. Klar, and P. Nurse. 1991. Molecular genetic analysis of fission yeast *Schizosaccharomyces pombe. Methods Enzymol.* 194:795–823. http://dx.doi.org/10.1016/0076-6879(91)94059-L

Nakada, C., K. Ritchie, Y. Oba, M. Nakamura, Y. Hotta, R. Iino, R.S. Kasai, K. Yamaguchi, T. Fujiwara, and A. Kusumi. 2003. Accumulation of anchored proteins forms membrane diffusion barriers during neuronal polarization. *Nat. Cell Biol.* 5:626–632. http://dx.doi.org/10.1038/ncb1009

Olivera-Couto, A., M. Graña, L. Harispe, and P.S. Aguilar. 2011. The eisosome core is composed of BAR domain proteins. *Mol. Biol. Cell*. 22:2360–2372. http://dx.doi.org/10.1091/mbc.E10-12-1021

Parton, R.G., and K. Simons. 2007. The multiple faces of caveolae. *Nat. Rev. Mol. Cell Biol.* 8:185–194. http://dx.doi.org/10.1038/nrm2122

Schuck, S., and K. Simons. 2004. Polarized sorting in epithelial cells: raft clustering and the biogenesis of the apical membrane. *J. Cell Sci.* 117:5955–5964. http://dx.doi.org/10.1242/jcs.01596

Schuck, S., W.A. Prinz, K.S. Thorn, C. Voss, and P. Walter. 2009. Membrane expansion alleviates endoplasmic reticulum stress independently of the unfolded protein response. *J. Cell Biol.* 187:525–536. http://dx.doi.org/10.1083/jcb.200907074

Seger, S., R. Rischatsch, and P. Philippsen. 2011. Formation and stability of eisosomes in the filamentous fungus *Ashbya gossypii. J. Cell Sci.* 124:1629–1634. http://dx.doi.org/10.1242/jcs.082487

Senju, Y., Y. Itoh, K. Takano, S. Hamada, and S. Suetsugu. 2011. Essential role of PACSIN2/syndapin-II in caveolae membrane sculpting. *J. Cell Sci.* 124:2032–2040. http://dx.doi.org/10.1242/jcs.086264

Shibata, Y., J. Hu, M.M. Kozlov, and T.A. Rapoport. 2009. Mechanisms shaping the membranes of cellular organelles. *Annu. Rev. Cell Dev. Biol.* 25:329–354. http://dx.doi.org/10.1146/annurev.cellbio.042308.113324

Sikorski, R.S., and P. Hieter. 1989. A system of shuttle vectors and yeast host strains designed for efficient manipulation of DNA in *Saccharomyces cerevisiae. Genetics*. 122:19–27.

Steed, E., M.S. Balda, and K. Matter. 2010. Dynamics and functions of tight junctions. *Trends Cell Biol.* 20:142–149. http://dx.doi.org/10.1016/j.tcb.2009.12.002

Strádalová, V., W. Stahlschmidt, G. Grossmann, M. Blazíková, R. Rachel, W. Tanner, and J. Malínsky. 2009. Furrow-like invaginations of the yeast plasma membrane correspond to membrane compartment of Can1. *J. Cell Sci.* 122:2887–2894. http://dx.doi.org/10.1242/jcs.051227

Verma, P., A.G. Ostermeyer-Fay, and D.A. Brown. 2010. Caveolin-1 induces formation of membrane tubules that sense actomyosin tension and are inhibited by polymerase I and transcript release factor/cavin-1. *Mol. Biol. Cell*. 21:2226–2240. http://dx.doi.org/10.1091/mbc.E09-05-0417

Walther, T.C., J.H. Brickner, P.S. Aguilar, S. Bernales, C. Pantoja, and P. Walter. 2006. Eisosomes mark static sites of endocytosis. *Nature*. 439:998–1003. http://dx.doi.org/10.1038/nature04472

Walther, T.C., P.S. Aguilar, F. Fröhlich, F. Chu, K. Moreira, A.L. Burlingame, and P. Walter. 2007. Pkh-kinases control eisosome assembly and organization. *EMBO J.* 26:4946–4955. http://dx.doi.org/10.1038/sj.emboj.7601933

Wanaski, S.P., B.K. Ng, and M. Glaser. 2003. Caveolin scaffolding region and the membrane binding region of SRC form lateral membrane domains. *Biochemistry*. 42:42–56. http://dx.doi.org/10.1021/bi012097n

Ziółkowska, N.E., L. Karotki, M. Rehman, J.T. Huiskonen, and T.C. Walther. 2011. Eisosome-driven plasma membrane organization is mediated by BAR domains. *Nat. Struct. Mol. Biol.* 18:854–856. http://dx.doi.org/10.1038/nsmb.2080

Ziółkowska, N.E., R. Christiano, and T.C. Walther. 2012. Organized living: formation mechanisms and functions of plasma membrane domains in yeast. *Trends Cell Biol.* 22:151–158. http://dx.doi.org/10.1016/j.tcb.2011.12.002